



**HAL**  
open science

## Automatic Detection and Classification of Defect on road Pavement using Anisotropy Measure

Tien Sy Nguyen, Manuel Avila, Stéphane Begot

► **To cite this version:**

Tien Sy Nguyen, Manuel Avila, Stéphane Begot. Automatic Detection and Classification of Defect on road Pavement using Anisotropy Measure. European Signal Processing Conference, 2009, Glasgow, United Kingdom. pp.617-621. hal-00666919

**HAL Id: hal-00666919**

**<https://hal.science/hal-00666919>**

Submitted on 6 Feb 2012

**HAL** is a multi-disciplinary open access archive for the deposit and dissemination of scientific research documents, whether they are published or not. The documents may come from teaching and research institutions in France or abroad, or from public or private research centers.

L'archive ouverte pluridisciplinaire **HAL**, est destinée au dépôt et à la diffusion de documents scientifiques de niveau recherche, publiés ou non, émanant des établissements d'enseignement et de recherche français ou étrangers, des laboratoires publics ou privés.

# AUTOMATIC DETECTION AND CLASSIFICATION OF DEFECT ON ROAD PAVEMENT USING ANISOTROPY MEASURE

*Tien Sy NGUYEN(1)(2), Manuel AVILA(1), BEGOT Stephane(1)*

(1) Institute PRISME  
University Orleans, IUT Chateauroux, France  
(2) Vectra Company, Buzanais, France  
web: [www.vectra.fr](http://www.vectra.fr)  
email: [tien-sy.nguyen@etu.univ-orleans.fr](mailto:tien-sy.nguyen@etu.univ-orleans.fr)

## ABSTRACT

Existing systems for automated pavement defect detection can only identify cracking type defects. In this paper, we introduce a method which can detect not only cracks as small as 1mm in width, but also two other defect types: joint and bridged. Road images are captured by our acquisition system. Firstly, a pre-processing step is applied on images to remove lane-marking. Then an anisotropy measure is calculated to detect road defects. Finally, a backpropagation neural network is used to classify the images into four classes: defect-free, crack, joint and bridged. Experimental results were performed on real road images which were labelled by human operators. Comparisons with other methods are also given.

## 1. INTRODUCTION

To manage road network, road authorities need accurate and up-to-date information about road defects. In France, thousands of kilometers of roads need to be inspected each year. In the past, road inspection process was done manually on road by human inspectors; this method is slow and unsafe for the inspectors and road users [1]. In the last few years, several automated pavement inspecting systems which use advanced machine vision technology have been developed. Some such devices are CSIRO's RoadCrack vehicle [2] and Roadware's ARAN system [3]. Unfortunately, all existing systems are only able to detect crack defects. We developed AMAC®[4] (Figure 1(a)) - a multifunction device for road analysis. One of its functions is to capture road surface images for defect inspection. Actually, the inspection process is done offline by human operators via viewing captured images. This manual inspection is not only time-consuming, costly but also subjective. For this reason, methods for automatic defect detection surface images are required.

Defect detection on pavement surface is a difficult problem due to the noisy pavement surfaces [5]. There are different types of texture that can be encountered on road pavements. Furthermore, by traffic effects, pavement texture varies on different zones of the image. Authors in [1] also showed that many road pavements have "strong texture". It means that, crack is thinner than aggregate size and distance inter-aggregates. As a result, it is difficult to distinguish a crack with an unusual aggregate distribution. Because of the above reasons, methods for detecting defects on texture surface which use regularities of background texture as frequency or orientation cannot be applied on road pavement surface.

All existing methods for detecting defect on pavement surface were based on characteristics of crack. They consider that crack pixels are darker than their surrounding. Authors in [6, 7, 8, 9, 10] used a fixed threshold, while Cheng et al [11] employed a fuzzy threshold technique to detect dark pixels (crack). Oliveira et al [12] and Huang [13] proposed another approach, they divide image into grid cells and each cell is classified as crack or crack-free cell using mean and variance of grayscale values. Subirats et al [1] supposed that, by applying a 2D CWT (Continuous Wavelet Transform), the differences between crack pixels and background pixels could be raised up. In their approach, crack pixels were identified by thresholding on coefficient maps of 2D CWT through different scales. But in case of "strong texture", the CWT not only raises up crack pixels but also raise noise.

From our experience in pavement image analyzing and by deduction from above researches, we found that crack has three characteristics:

- Darker than its surrounding (because of crack form, many light rays cannot be reflected from crack to camera (Figure 1(b)),
- Continuous (crack can be thinner than aggregates but it is always longer than them),
- Dominant orientation (on all length of crack or on each segment).

Crack detection approaches, which use only the first feature, have limitations on difficult texture type of pavement. Cell-dividing methods are only able to detect big crack. When crack is small ( 1 or 2 pixels in width), cell-dividing methods cannot distinguish crack-cell and normal - cell by only considering mean and variance of the cell. Threshold method has drawbacks on dark textures and on low contrast cracks [6].

In this paper, we introduce a crack detection method using an anisotropy measure. This measure takes into account all of three above crack features. Our experimental results show that the method gives a good crack detection on several pavement types. Crack which is as small as one millimeter in width can be detected. Furthermore, two other types of defect (joint and bridged) which have similar features as crack can be detected by our method.

In the next sessions, after a brief description of our acquisition system, we describe our defect detection and classification method. Experimental results are presented in comparison with other methods and with the results of operator detection. Finally, conclusions are given.

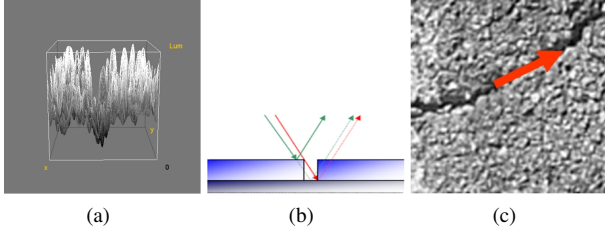


Figure 1: Crack analysis: 3D profile (a), illumination model on a crack (b), dominant orientation (c)

## 2. IMAGE ACQUISITION SYSTEM

The vehicle continuously captures road images (each 4 meters by 4 meters) as it travels at an average speed of 80 kilometers per hour. Captured image size is 4096x4096 and its resolution is 1mm per pixel, 8 bits grayscale. Image acquisition is performed with two line scan cameras mounted at an angle of approximately 30 degrees to road surface, captured regions are illuminated by two laser illuminators (Figure 2(b)), therefore, light condition has almost no effect on the quality of acquired images [6].

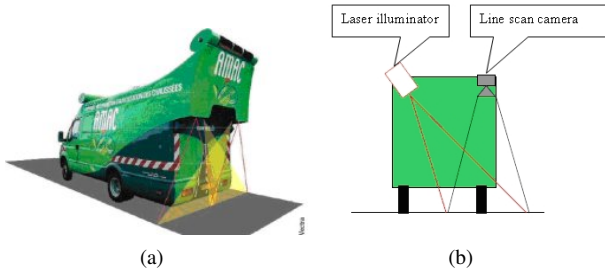


Figure 2: Our road image acquisition system: Vehicle AMAC®(a), image acquisition system of AMAC®(b)

## 3. CRACK DETECTION AND CLASSIFICATION METHOD

In this part, we describe our automatic defect detection method. We divide the method into three steps. First step is to detect position of lane-marking. In second step, defect is detected by calculation of anisotropy. The last step is to classify defect using different defect features extracted from the second step.

### 3.1 Lane-marking detection

Thanks to the constant illumination of two laser illuminators, we don't need to normalize captured image as it was done in [11, 13]. Another problem remaining before crack detection is road lane-marking. Lane-marking contours could be detected as a defect. Detecting lane markings also become critical to determine location of defects. On images captured by AMAC®system, lane marking is not occluded and have a high value of greyscale level. To detect lane marking, firstly, we applied a threshold to get a binary image of white pixels (the pixels which have value greater than a threshold  $thr_{lm}$ ). Then we used Probabilistic Hough Transform [15] to detect lines on this binary image. Lane-markings were de-

tected from these lines in consideration to their orientations and their dimensions. An example of lane-marking detection is shown in Figure. 3

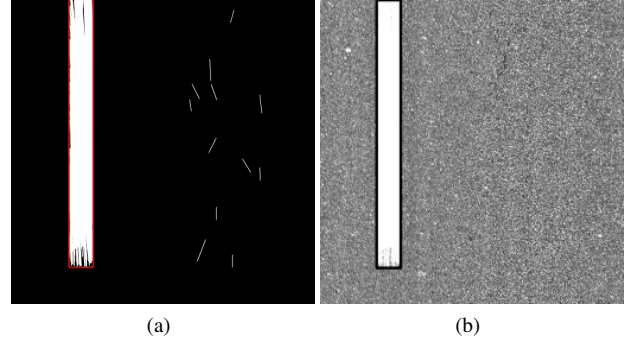


Figure 3: Lane-marking detection on a road image: Lines detection by Hough transforms (a), lane-marking detection result (b)

If any lane-marking is present in the inspected image, its region (e.g. the black rectangular in Figure 3(b)) will not be considered in the defect detection. The lane-marking pixels are not taken into account to calculate global information of the image.

### 3.2 Defect detection based on Texture Anisotropy

#### 3.2.1 Definition of Conditional Texture Anisotropy

Conditional Texture Anisotropy (CTA) was first introduced by F. Roli in [15]. The main idea is to find out a measure which takes small value in one orientation (e.g. along the orientation of crack) and takes big value in other orientations. The CTA of a pixel  $l$  was defined as:

$$CTA(X^l) = \frac{\max_j \{p(x_j^l/l \in w_1)\} - \min_j \{p(x_j^l/l \in w_1)\}}{\max_j \{p(x_j^l/l \in w_1)\}} \quad (1)$$

Where:

- $X^l = (x_1^l, x_2^l, \dots, x_m^l)$  is feature vector of pixel  $l$ . Each pixel  $l$  is characterized by a set of  $n$  features and each feature is compute along  $m$  orientations.
- $x_j^l = (feature\_1_j^l, feature\_2_j^l, \dots, feature\_n_j^l)$ ,  $j = 1 \dots m$  is sub-vector of  $X^l$  representing  $n$  features computed along orientation  $j$ .
- Pixels in an inspected image are divided into two classes: defect-free pixels class  $w_1$  and defective pixels class  $w_2$ .
- $p(x_j^l/l \in w_1)$  is the conditional probability of pixel  $l$  belong to defect-free pixels class  $w_1$  along orientation  $j$ . According to crack characteristics, if  $k$  is the dominant orientation of a crack (Figure 1(c))  $p(x_k^l/l \in w_1)$  will take low value for pixels belonging to this crack. As well  $p(x_j^l/l \in w_1)$  will take high values for other orientations  $j \neq k$ .

We can deduce from equation 1 that CTA takes values in range  $[0, 1]$ . CTA value is close to 0 for defect free pixel. At crack pixel, CTA takes high value (close to 1) because features extracted along crack orientation are very different from other orientations.

### 3.2.2 Crack detection by CTA

According to crack characteristics on road surface images, we chose mean and standard deviation as two features for calculating CTA. The calculation method is presented as follows:

- $2 * d + 1$  is the length of a line, along which we calculate each feature (Figure 4(a)).
- Four orientations  $0^\circ$ ,  $45^\circ$ ,  $90^\circ$  and  $135^\circ$  were considered.
- Two features were used: mean  $m_j^l$  and standard deviation  $\sigma_j^l$  of  $2 * d + 1$  pixels along considered orientation  $j$ .

Feature vector of pixel  $l$  along orientation  $j$  is :

$$x_j^l = (m_j^l, \sigma_j^l) \quad (2)$$

To evaluate the pre-assumed probability of a pixel  $l$  to be “a defect-free pixel in one orientation  $j$ ” we calculated:

$$p(x_j^l / l \in w_1) = \frac{D - \Delta_j}{D} \quad (3)$$

$m$  and  $\sigma$  are calculated on the whole image (except lane-marking pixels). Equation (3) can be compared with a normalized distance which is close to 1 for defect-free pixel. Mean and standard deviation along each defect-free orientation are “near” global values. In case of crack pixel, distance  $\Delta_k$  along the dominant orientation  $k$  of defect increases and  $p(x_k^l / l \in w_1)$  decreases towards zero. CTA is then calculated as in equation (1) by using  $p(x_j^l / l \in w_1)$  defined in equation (3). It is worth noting that  $p(x_j^l / l \in w_1)$  is a pre-assumed probability value used for calculating CTA. We don’t detect defects by using this pre-assumed probability but by calculating CTA. The information which plays the most important role for defect detection is the distribution of mean and standard deviation values along different orientations.

Figure 4 illustrates a calculation of CTA on two pixels: crack pixel  $l_1$  and defect-free pixel  $l_2$ . With pixel  $l_1$ , values of  $(m_j^l, \sigma_j^l)$  along 4 orientations are: (99.12,47.55), (93.7,34.50), (37.9, 14.39) and (104.77,39.45).  $(m_j^l, \sigma_j^l)$  of image is (123.58, 48.13). CTA of  $l_1$  is **0.64**. With pixel  $l_2$ , values of  $(m_j^l, \sigma_j^l)$  along 4 orientations are: (111.97, 36.01), (108.95, 25.84), (110.52, 33.46), (116.05, 29.60). CTA of  $l_2$  is **0.08**.

Figure 5 shows us the evolution of CTA on  $l_1$  and  $l_2$  (Figure 4.b) by different lengths  $d$ . The inspected road is a bituminous concrete, whose aggregate maximum size is 12 mm. In order to CTA can distinguish crack pixels from noise pixels,  $d$  needs to be chosen to ensure that  $2 * d + 1 \gg \gg$  aggregate size. There are several pavement types but their maximum aggregate size are always much smaller than crack length. So  $d$  is chosen in manner that  $2 * d + 1$  is greater than maximum aggregate size of all pavement types. As a result, the method is stable to variations of pavement types. As we can see in figure 5, all  $d$  length from 8 pixels to 38 pixels can be used to make a big difference of CTA value on crack pixels and on defect-free pixels.

When CTA image (image which represent computed CTA values) is computed, CTA of crack pixels are much greater than defect-free pixels (Figure 6 (b)). Thus, crack pixels (Figure 6 (c)) are easily detected by a threshold from CTA image.

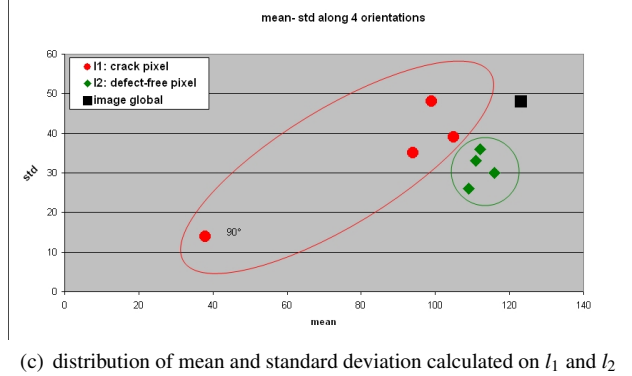
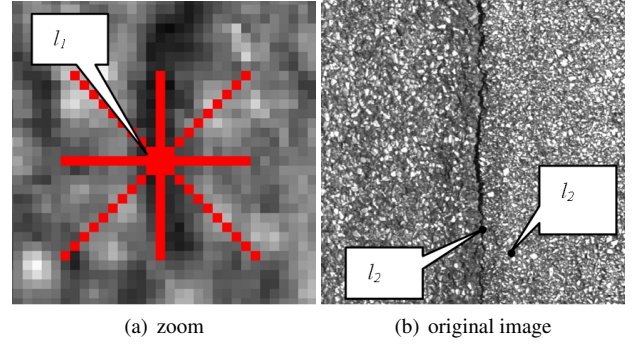


Figure 4: Example of CTA on two pixels: crack pixel  $l_1$  and crack-free pixel  $l_2$  with  $d = 14$ .

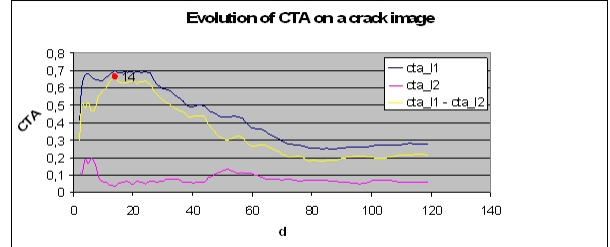


Figure 5: CTA evolution on pixel  $l_1$  and  $l_2$  by varying  $d$ .

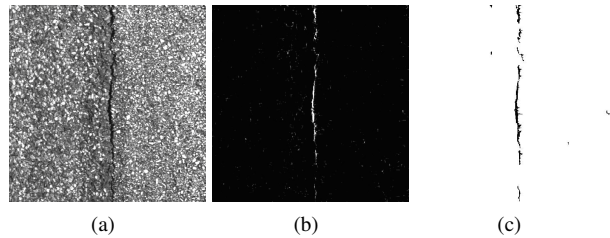


Figure 6: Crack detection example: Original images (a), CTA image result (CTA values were converted scale from [0,1] to [0,255] grey level ) (b). Crack detection result (c)

### 3.2.3 Joint and bridged detection

Two other defects: joint and bridged are also very common on road. Joints (Figure 7(a,b)) have all three characteristics of cracks. Therefore, joint can be detected by using CTA with a higher value of  $d$ . ( $d$  must be greater than joint width to ensure that mean and standard deviation calculated on

dominant orientation are different from other orientations). Bridged defects (Figure 7(c,d)) is similar to background but their contours have two characteristics: continuity and dominant orientation. Our method can detect bridged contours and then bridged defect (Figure 10).

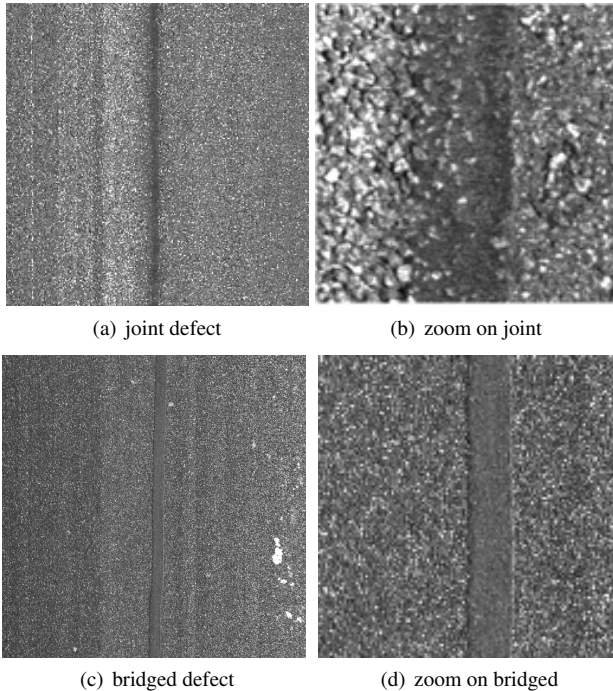


Figure 7: Joint and bridged defect example.

### 3.3 Features extraction

We regrouped defect pixels detected from the above steps into connected regions. Then we apply a “close” succeed by an “open” morphological operations [6] to connect the close pixels and to remove small regions which are considered as noise. Remaining regions should be:

- Crack(Longitudinal, transversal or alligator),
- Joint,
- Bridged contour,
- Defect-free region but by effect of traffic, this region is aligned.

We noticed that:

- + Cracks have a lowest value of mean and standard deviation.
- + Joint is darker than a bridged contour. Joint is much higher than crack and bridged contour.
- + Bridged contours separate two different regions.

Five features were extracted from each connected region to classify them:

- \* Mean (with pixel values are taken from original image)
- \* Standard deviation.
- \* Width of boundary rectangle.
- \* Difference of mean and standard deviation of two cells at two sides of the connected region.

Each above feature is normalized by its maximum to take value from 0 to 1 (mean and standard deviation is normalize with 255; width is normalized with the diagonal of image).

### 3.4 Defect classification

To classify defect, we used a multi-layer perceptrons neural network (MLPNN), the most commonly used type of neural networks. MLPNN consists of the input layer, output layer and one or more hidden layers. Each layer of MLP includes one or more neurons that are directionally linked with neurons from previous and next layer [16]. We chose a MLP with two hidden layers for our application. Five neurons in input layer correspond to 5 above features and 4 neurons in output layer correspond to 3 defect classes and one defect-free class. The MPLPNN was trained with back-propagation algorithm. We selected training images from different defect (and defect-free) images on different pavement types. The training set was chosen from images captured during year 2007. For test we use images captured during year 2008. The training set contains 150 defect free images, 100 longitudinal crack images, 87 transversal crack images, 35 alligators crack images, 100 joints and 100 bridgeds.

## 4. EXPERIMENTAL RESULTS

Because small crack cannot be seen in reduce images, we will present results of crack detection on a sub region of full-size images.

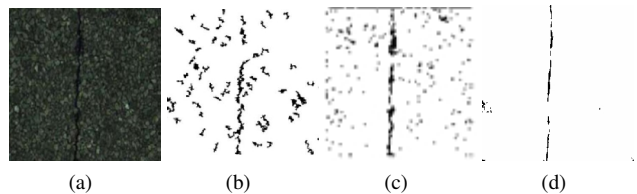


Figure 8: Comparison of our method with threshold method [6] and Subirat's 2D wavelet transform method [1] on a “strong texture” image ,  $d = 14$ : inspected image (a), Subirat's method (b), threshold method (c), our method CTA (d)

Comparative results of our method with threshold method [6] and Subirat's 2D CWT method [1] are shown in Figure 8. The 2D wavelet transform raises the crack but it raises up also noise because the continuity was not considered (Figure 8(b)). On the other hand, our method only raises the continuous crack pixels. The threshold method (Figure 8(c)) has limitations because it cannot differentiate a dark pixel of defect-free texture from a crack pixel.

In Figure 9. We show detection result on defect image of joint type. Our method can detect this type of defect with “high” value of  $d$  ( in this example,  $d = 28$ ).

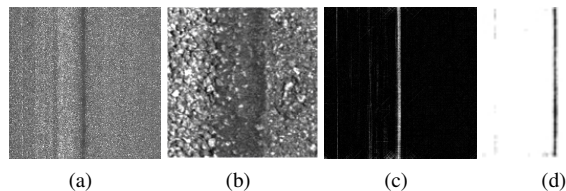


Figure 9: Result on an image with joint defect,  $d = 28$ : inspected image (a), zoom (b), CTA image (c), defect detection (d)

Results of detection on a bridged image are shown in Figure 10, as bridged are similar to background texture, they are

detected via detection of bridged contours.

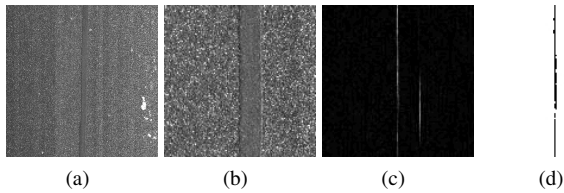


Figure 10: Result on an image with bridged defect,  $d = 14$ : inspected image (a), zoom (b), CTA image (c), defect detection (d)

Detection and classification results on a real road image set are presented in table 1. This set was selected from images captured during year 2008. We tried to collect images with different pavement types and different defect type (variation of width, length and orientation of each defect type). Results on this set show that our method provides a very good detection on cracks and joints. Cracks as small as 2 mm (1 mm = 1 pixel) can be detected, even the "well" continuous cracks as small as 1 mm can be detected. The seven undetected cracks are composed of a set of very small and discontinuous segments. Results on bridgeds are not as good as results on cracks and joints. As some bridgeds are too similar to background, its contours cannot be detected or our method cannot distinguish these bridgeds with other aligned regions on road surface. Aligned regions are also the reason for 6% wrong detection on defect-free images.

Image type	Number of images	Errors	Percentage of good detection (%)
Defect-free	200	8	96
Crack	271	7	97.4
Joint	235	0	100
Bridged	203	18	91.13

Table 1: Detection and classification result on a real road image set

## 5. CONCLUSION

In this paper, we introduced a method for defect detection on road surface images. Our method can detect three defect types: cracks, joints and bridged. The method use a measure of Conditional Texture Anisotropy (CTA) to detect defects on images and then use a multi-layer perceptron neural network to classify detected defect into three defect types: cracks, joint and bridged. The classification of defect can also correct the wrong detection of a defect-free image by classifying it to defect-free class. Unlike other methods that only considered one characteristic of crack, our method use CTA which takes into account all three features of crack. The comparison results of our method with other methods show the efficiency of our method and justify our choice.

Further more, to improve the performance of the neural network in classification of defect to data outside of training set (new type of road pavement). We plant to implement a retrainable neural network [17] which can adapt the trained neural network to the current data.

## REFERENCES

- [1] P. Subirats, J. Dumoulin, V. Legeay and D. Barba, "Automation of Pavement Surface Crack Detection using the Continuous Wavelet Transform" in *Proc. IEEE International Conference on Image Processing ICIP*, 2006, pp. 3037-3040.
- [2] CSIRO, RoadCrack Specifications.
- [3] Roadware Group Inc, Wisecrax data sheet.
- [4] Vectra's AMAC® specifications.
- [5] H. Lee, "Application of machine vision techniques for the evaluation of highway pavements in unstructured environments" in *Proc. Fifth International Conference on Advanced Robotics 'Robots in Unstructured Environments'*, 1991, pp 1425-1428 vol.2
- [6] N. T. Sy, M. AVILA, S. Begot and J. C. Bardet, "Detection of defects in road surface by a vision system," in *Proc. 14th IEEE Mediterranean Electrotechnical Conference MELECON*, 2008, pp. 847-851.
- [7] S. Nallamothu and K. Wang, "Experimenting with recognition accelerator for pavement distress identification," in *Transport Research Record*, 1996. pp. 130-135.
- [8] V. K. Kalikiri, N.W. Garrick, and L.E.K. Achenie, "Image processing methods for automated distress evaluation," in *Transportation research record* 1994. 1435: p. 45-51.
- [9] K. M. Chua and L. Xu, "Simple procedure for identifying pavement distresses from video images" in *Journal of transportation engineering*, 1994. 120: p. 412-431.
- [10] D. Jean et al, "Dtection de fissures de surface de chaussées par technique d'imagerie dans le visible" in *Journes des Sciences de l'Ingénieur*, 2003.
- [11] H. D. Cheng et al, "Novel approach to pavement cracking detection based on fuzzy set theory" in *Journal of Computing In civil Engineering*, 1999. 13(4): p. 270-280.
- [12] H. Oliveira and P. Lobato Correia, "Identifying and retrieving distress images from road pavement surveys" in *Proc. 15th IEEE International Conference on Image Processing ICIP*, 2008, 57-60.
- [13] H. Yaxiong, X. Bugao, "Automatic inspection of pavement cracking distress" in *Journal of Electronic Imaging*, 2006, 15(1): 013017-1 013017-6.
- [14] J.R. Bergen and H. Shvaytser, "A probabilistic algorithm for computing Hough Transforms" in *Journal Of Algorithms*, 12(4):639-656, 1991
- [15] F. Roli, "Measure of texture anisotropy for crack detection on textured surfaces" in *Electronics Letters*, 1996, 32, 1274-127
- [16] Intel OpenCv Reference
- [17] A. D. Doulamis et al, "On-Line Retractable Neural Networks: Improving the Performance of Neural Networks in Image Analysis Problems" in *IEEE Trans. on Neural Networks*, vol. 11, No. 1, january 2000.